Mitigation of transverse single-bunch instabilities with longitudinal impedance, feedback, and chromaticity

Liwei Pan,[1,2] Yuan Zhang,[1,2,*] Kazuhito Ohmi,[1,3] Chuntao Lin,[1] Na Wang,[1] Yuzhe Liu,[1,2] and Siyuan Feng[1,2]

[1]*IHEP, Institute of High Energy Physics, Yuquan Road, Beijing 100049, China*
[2]*University of Chinese Academy of Sciences, Yuquan Road, Beijing 100049, China*
[3]*KEK, High Energy Accelerator Organization, Tsukuba, Ibaraki 305-0801, Japan*

(Received 10 January 2026; accepted 15 April 2026; published 15 May 2026)

In this paper, we investigate methods for suppressing transverse single-bunch instability. A theoretical framework incorporating longitudinal impedance, feedback, and chromaticity is presented. Our results show that the combined action of these effects effectively suppresses the transverse single-bunch instability. The instability threshold can be raised by a factor of 2 or more relative to I_{tmci}, defined as the threshold under transverse impedance only. The key stabilization mechanism arises from two effects: feedback and positive chromaticity cause the instability to be dominated by nonzero-order azimuthal modes, while longitudinal impedance introduces a significant tune spread in these modes. This stabilization mechanism, however, is ineffective in the negative chromaticity regime. The theory is applied to three electron storage rings: SuperKEKB, CEPC, and HEPS. Both the analysis and simulation lead to consistent conclusions.

DOI: 10.1103/1kpk-757b

I. INTRODUCTION

The transverse single-bunch instabilities driven by coupling impedance can limit beam quality and even lead to beam loss in synchrotrons. Therefore, researchers have long tried to find ways to suppress these instabilities [1–3]. One of the most serious is the transverse mode coupling instability (TMCI) with a clear intensity threshold. Finding ways to control TMCI remains an important research goal. Chromaticity has been explored as a mitigating method for TMCI. However, this does not always work within a reasonably attainable value [4]. Another method is the bunch-by-bunch feedback [5]. Unfortunately, feedback systems can introduce a destabilizing effect, called ITSR instability [6] or −1 mode instability [7]. Another idea is to combine the beneficial effects of both chromaticity and feedback. Some theoretical works have shown that using feedback combined with negative chromaticity can significantly increase the instability threshold [8,9]. This can be thought of as a superposition of two separate effects [10]: feedback suppresses the oscillations of the bunch's lowest-order head-tail mode, while negative chromaticity stabilizes the higher-order head-tail modes. Together, they stabilize all modes. However, Smaluk *et al.* highlighted a conflict between theoretical predictions and machine experimental results [11]. It was concluded that the combination of feedback and positive chromaticity is generally a better choice in practice [12]. About two decades ago, it was found that longitudinal impedance helps to damp transverse instability with high chromaticity in ESRF [13]. Recent simulations in FCC-ee provide indications that the longitudinal impedance affects transverse instability threshold significantly [14–16]. In early theoretical work, longitudinal impedance was not self-consistently incorporated into the theoretical framework for transverse instabilities. Smaluk *et al.* accounted for the intensity-dependent bunch lengthening [12]. Kernel *et al.* incorporated the synchrotron frequency spread induced by longitudinal impedance [13]. Both approaches yielded results consistent with their experimental data. Xu *et al.* systematically investigated the influence of longitudinal impedance on TMCI [17] in both analysis and simulation. They demonstrated that the incoherent synchrotron tune spread induced by longitudinal impedance lowers the instability threshold.

Several other mitigation strategies are also worth mentioning. In the CERN SPS, modifying the machine optics to operate farther from transition has been shown to increase the instability threshold by approximately a factor of 2 [18]. In the presence of transverse feedback at zero chromaticity, it is possible to exploit transverse Landau damping, as the required amount of it is rather small [6]. Furthermore, in the presence of significant stability asymmetry, transverse linear coupling can be introduced to suppress the instability

*Contact author: zhangy@ihep.ac.cn

Published by the American Physical Society under the terms of the Creative Commons Attribution 4.0 International license. Further distribution of this work must maintain attribution to the author(s) and the published article's title, journal citation, and DOI.

[19]. In proton machines, space charge also exerts a significant influence on the TMCI threshold [20].

In this paper, we present a transverse mode-coupling theory that incorporates longitudinal impedance, ideal feedback, and chromaticity, and discuss how the interplay among these effects can be exploited to mitigate TMCI. The theoretical formulation is presented in Sec. II. In Sec. III, we compute variations in the instability threshold across a broad parameter space using both simulation and analytical methods on three machines: SuperKEKB, CEPC, and HEPS. This broad parameter-space survey allows us to reconcile discrepancies found in previous studies. Since the underlying physics for all three is consistent, Sec. IV uses SuperKEKB as a representative case to demonstrate variations in eigenmodes with different parameter settings, thereby providing a clear physical picture. Finally, Sec. V summarizes our findings and provides recommendations for designing and operating future electron storage rings.

II. THEORY DERIVATION

We study the stability of the dipole amplitudes using an eigenvalue problem. This method was first introduced by Ohmi *et al.* in Ref. [21] to analyze a coherent beam-beam mode. The dipole oscillation in the longitudinal phase space is expressed by the dipole amplitudes $y(J,\phi;t)$ and $p_y(J,\phi;t)$ in the longitudinal action-angle phase space (J,ϕ)

$$y(J,\phi;t)=\int dydp_y y\Psi(y,p_y,z,\delta;t), \tag{1}$$

where $\Psi(y,p_y,z,\delta)$ is the four-dimensional phase space distribution of the beam particles. The longitudinal distribution discussed above is $\psi(J,\phi)=\int\Psi dydp_y$. The dipole amplitude is expanded into azimuthal and radial modes as

$$\begin{aligned} y(J,\phi;t)&=\sum_{l=-l_{\max}}^{l_{\max}} y_l(J;t)e^{il\phi},\\ p_y(J,\phi;t)&=\sum_{l=-l_{\max}}^{l_{\max}} p_l(J;t)e^{il\phi}, \end{aligned} \tag{2}$$

where the azimuthal mode is truncated by $l_{\max}$. The radial coordinate J is discretized with a step of ΔJ. The length of the vector $y_l(J;t)$ and $p_l(J;t)$ is $(2l_{\max}+1)n_J$, where J is discretized into n_J steps. The stability for each radial and azimuthal mode is treated as an eigenvalue problem of a square matrix of size $[2(2l_{\max}+1)n_J]^2$, as formulated by Kuroo *et al.* in Ref. [22]. The method was further extended by Lin *et al.* in Ref. [23] to account for potential well distortion.

Regarding chromaticity, two approaches are considered: The first uses a transfer/revolution matrix for (y,p_y) that includes a tune shift as a function of δ, where $\delta=\Delta P/P_0$ is relative momentum error. The transfer matrix consists of four submatrices of size $[(2l_{\max}+1)n_J]^2$, which transfer (y,p_y) after one revolution. The four submatrices are not diagonalized due to the chromaticity. The second method utilizes eigenvectors for azimuthal mode numbers by introducing the head-tail phase, as described in Ref. [24]. In this case, the submatrices are diagonalized, just as those without chromaticity. In this work, we employ the first method. The difference between the two is not essential for solving the eigenvalue problem, and both yield identical results.

When the impedance (here including the feedback kicker) is distributed along the ring, it is sufficient to examine the tune of each radial and azimuthal mode, as shown in Ref. [25]. In this scenario, the matrix size reduces to $[(2l_{\max}+1)n_J]^2$. Both the matrix approach and the tune shift method produce consistent results when the tune is far from synchro-beta resonances, as demonstrated in Ref. [25].

A. Processing of longitudinal phase space

We choose $s=z+ct$, representing the length measured along the closed orbit from an initial point, as the timelike variable. c is the speed of light and t is clock time. z is used as the longitudinal coordinate, representing the distance from the synchronous particle, and $z>0$ represents ahead of it.

When a bunch travels through the accelerator beam pipe, the leading particles generate electromagnetic fields that act on trailing particles. These longitudinal electromagnetic interactions are described as the longitudinal wakefield. The effect of the longitudinal wakefield can be written as a momentum kick [1]

$$\Delta\delta(z)=-\frac{4\pi\epsilon_0 N_b r_0}{\gamma}\int_{-\infty}^{\infty} W^{\parallel}(z-z')\rho(z')dz', \tag{3}$$

where r_0 is the classical particle radius, ϵ_0 is the vacuum dielectric constant, N_b is the bunch particle number, γ is the relativistic factor, $W^{\parallel}(z)$ is the longitudinal wakefield function, and $\rho(z)$ is the normalized line density. In this paper, we choose the SI unit.

Considering the effect of longitudinal wakefield, the longitudinal normalized Hamiltonian of the particle can be written as [23,26]

$$\begin{aligned} H&=\frac{\delta^2}{2\sigma_\delta^2}+\frac{z^2}{2\sigma_z^2}-\frac{1}{\eta C_0\sigma_\delta^2}\frac{4\pi\epsilon_0 N_b r_0}{\gamma}\\ &\quad\times\int_{-\infty}^{z}dz''\int_{-\infty}^{+\infty}dz'W^{\parallel}(z''-z')\rho(z')\\ &=\frac{\delta^2}{2\sigma_\delta^2}+V_{\mathrm{PW}}(z), \end{aligned} \tag{4}$$

where $V_{\mathrm{PW}}(z)$ is the total potential well, C_0 is the ring circumference, η is the slip-phase factor, σ_z is the rms

bunch length, and σ_δ is the rms energy spread. Equation (4) reveals a gradual deformation of the potential well from the initial rf potential as the bunch intensity rises. The density $\rho(z)$ should be numerically calculated using the Haïssinski equation [27]

$$\rho(z) = \rho_0 \exp\left[-\frac{z^2}{2\sigma_z^2} + \frac{4\pi\epsilon_0 N_b r_0}{\eta\sigma_\delta^2 C_0 \gamma}\int_{-\infty}^{z} dz'' \times \int_{-\infty}^{+\infty} dz' W^{\parallel}(z''-z')\rho(z')\right]. \tag{5}$$

The method to solve Eq. (5) is not discussed here because it has been presented in many previous publications [28–30].

To take advantage of the periodicity in the system, transforming the $z-\delta$ coordinates into action-angle coordinates proves to be an effective way [31,32]. The orbits are distorted under the effect of the longitudinal wakefield. Kicsiny *et al.* [33] tried to linearize the wakefield term in Eq. (4). However, as the intensity increases, the head-tail asymmetry becomes sufficiently strong to invalidate the linear approximation. Here we adopt the more self-consistent method presented in Ref. [23]. For each specific orbit, using the Hamiltonian in Eq. (4), we could derive the action J

$$J(H) = \frac{1}{2\pi}\oint \delta\, dz = \frac{1}{\pi}\int_{z_{\min}}^{z_{\max}} dz\sqrt{2\sigma_\delta^2[H - V_{\mathrm{PW}}(z)]}, \tag{6}$$

where $z_{\min}$ and $z_{\max}$ correspond to the left and right turning points of the J-constant phase-space orbit. To derive the ϕ, the second type generating function $F_2(z,J) = \tilde{F}_2(z, H(J))$ should be used. Using the property of generating function of $\delta = \partial F_2(z,J)/\partial z$ and the expression of δ in Eq. (4), we can get

$$\phi(z,J) = \frac{\partial F_2(z,J)}{\partial J} = \frac{\partial \tilde{F}_2(z,H(J))}{\partial J} = \frac{\partial}{\partial J}\int_{z_{\min}}^{z} dz'\sqrt{2\sigma_\delta^2(H(J) - V_{\mathrm{PW}}(z))}. \tag{7}$$

Because of the distortion of longitudinal phase space, the synchrotron tune ν_s becomes a function of J. The calculating method is shown in [23,26]. Obviously, Eqs. (4), (6), and (7) can only be calculated numerically.

Based on $\phi(z,J)$ in Eq. (7), we can get $z(J,\phi)$ numerically. By combining Eq. (4), with $z(J,\phi)$, $\delta(J,\phi)$ is obtained numerically. The line density of δ keeps Gaussian $\exp(-\delta^2/2\sigma_\delta^2)/(\sqrt{2\pi}\sigma_\delta)$. The whole longitudinal probability density can be written as

$$\psi(J,\phi) = \psi(z(J,\phi),\delta(J,\phi)) = \rho(z(J,\phi))\frac{1}{\sqrt{2\pi}\sigma_\delta}\exp(-\delta(J,\phi)^2/2\sigma_\delta^2) \tag{8}$$

$\psi(J,\phi)$ is stationary below the microwave instability threshold. In this situation, probability density ψ is a function only related to J. Therefore, Eq. (8) can be integrated as

$$\int_0^{2\pi}\psi(J,\phi)d\phi = 2\pi\psi(J). \tag{9}$$

Now we have numerically obtained four key functions: $z(J,\phi)$, $\delta(J,\phi)$, $\psi(J)$, and $\nu_s(J)$. These are all necessary in the following steps. We can also construct $V_{\mathrm{PW}}(z)$ in Eq. (4) from longitudinal impedance $Z^{\parallel}(\omega)$

$$-\frac{1}{\eta C_0\sigma_\delta^2}\frac{2\epsilon_0 N_b r_0}{\gamma}\int_{-\infty}^{+\infty} d\omega Z^{\parallel}(\omega) \times \int_{-\infty}^{z} dz''\cdot e^{i\omega z''/c}\int_{-\infty}^{+\infty} dz'\cdot\rho(z')e^{-i\omega z'/c}, \tag{10}$$

where i is the imaginary unit, and ω is the angular frequency.

B. Arc transfer map

If the betatron tune is selected to avoid dangerous resonance lines, the synchro-betatron motion in the arc section can be described as a phase advance in transverse phase space. In this part, we adopt the approach presented in Ref. [34]. Assuming that the betatron tune is ν_0 and the linear chromaticity is ν_1, and the total tune is $\nu_y = \nu_0 + \nu_1\delta$. The amplitude-dependent tune shift is ignored. The betatron phase advance of a single turn can be written as

$$\mu(J,\phi) = 2\pi\int_0^1 dt\{\nu_0 + \nu_1\delta[J,\phi + 2\pi\nu_s(J)t]\}. \tag{11}$$

We normalize (y, p_y) by Twiss parameters, $Y = y/\sqrt{\beta_y}$ and $P = (\beta_y p_y + \alpha_y y)/\sqrt{\beta_y}$. Thus, after passing through the entire arc section, we have

$$\begin{aligned} Y_{n+1}[J,\phi+2\pi\nu_s(J)] &= \cos\mu(J,\phi)\cdot Y_n(J,\phi) + \sin\mu(J,\phi)\cdot P_n(J,\phi), \\ P_{n+1}[J,\phi+2\pi\nu_s(J)] &= -\sin\mu(J,\phi)\cdot Y_n(J,\phi) + \cos\mu(J,\phi)\cdot P_n(J,\phi), \end{aligned} \tag{12}$$

where $Y(J,\phi)$ and $P(J,\phi)$ describe the normalized dipole amplitude distribution in longitudinal phase space. n and

$n+1$ mean before and after the transformation. We expand $Y(J,\phi)$ and $P(J,\phi)$ to the summation of azimuthal modes

$$\begin{aligned} Y_n(J,\phi) &= \sum_l Y_{n,l}(J)e^{il\phi}, \\ P_n(J,\phi) &= \sum_l P_{n,l}(J)e^{il\phi}, \\ Y_{n+1}[J,\phi+2\pi\nu_s(J)] &= \sum_l Y_{n+1,l}(J)e^{il\phi+il2\pi\nu_s(J)}, \\ P_{n+1}[J,\phi+2\pi\nu_s(J)] &= \sum_l P_{n+1,l}(J)e^{il\phi+il2\pi\nu_s(J)}, \end{aligned} \tag{13}$$

where the summation index l is the azimuthal mode index, ranging from $-\infty$ to $+\infty$. This is possible because Y and P retain their periodicity with respect to ϕ even in a distorted longitudinal phase space. Then multiplying by $\exp[-il\phi - il2\pi\nu_s(J)]$ and integrating over ϕ for both sides of Eq. (12), yields

$$\begin{aligned} Y_{n+1,l}(J) &= e^{-il2\pi\nu_s(J)}\sum_{l'} A_{ll'}(J)Y_{n,l'}(J) \\ &\quad + e^{-il2\pi\nu_s(J)}\sum_{l'} B_{ll'}(J)P_{n,l'}(J), \\ P_{n+1,l}(J) &= -e^{-il2\pi\nu_s(J)}\sum_{l'} B_{ll'}(J)Y_{n,l'}(J) \\ &\quad + e^{-il2\pi\nu_s(J)}\sum_{l'} A_{ll'}(J)P_{n,l'}(J), \end{aligned} \tag{14}$$

where

$$\begin{aligned} A_{ll'}(J) &= \frac{1}{2\pi}\int_0^{2\pi} e^{i(l'-l)\phi}\cos\mu(J,\phi)d\phi, \\ B_{ll'}(J) &= \frac{1}{2\pi}\int_0^{2\pi} e^{i(l'-l)\phi}\sin\mu(J,\phi)d\phi. \end{aligned} \tag{15}$$

Next, we process the radial mode. We can use any complete orthogonal function system. Ideally, one would choose an orthogonal basis that ensures good physical convergence; however, if such a prospect is unclear, discretization in terms of J is meaningful in the sense that it allows representation of all functional degrees of freedom. Since neither $\delta(J,\phi)$ nor $\nu_s(J)$ has an analytical expression, we adopt the discretization method proposed by Oide and Yokoya [31,32], which employs a set of piecewise step functions as the orthogonal basis in the radial direction. In this way, the J axis is uniformly or nonuniformly decomposed into step functions of length ΔJ_k centered at J_k, where k indexes each function in order. The transfer matrix for the vector $[Y_l(J_k), P_l(J_k)]$ in the arc section can be written as

$$M_{\text{arc}} = e^{-il2\pi\nu_s(J_k)}\begin{bmatrix} A_{ll'}(J_k) & B_{ll'}(J_k) \\ -B_{ll'}(J_k) & A_{ll'}(J_k) \end{bmatrix}. \tag{16}$$

C. Transverse wakefield

Similar to the longitudinal wakefield, the transverse wakefield effects can also be described as momentum kicks. The mathematical treatment has been derived in Refs. [23,34,35]. The kick coming from the transverse wakefield $W^{\perp}$ can be expressed as

$$\begin{aligned} \Delta p_y(z) = -\frac{4\pi\epsilon_0 N_b r_0}{\gamma}\iint dz'd\delta'\psi(z',\delta')y(z',\delta') \\ \times W^{\perp}(z-z'). \end{aligned} \tag{17}$$

Using the normalized coordinates, Eq. (17) becomes

$$\begin{aligned} \Delta P_y(z) = -\frac{4\pi\epsilon_0 N_b r_0\beta_y}{\gamma}\iint dz'd\delta'\psi(z',\delta') \\ \times Y(z',\delta')W^{\perp}(z-z'). \end{aligned} \tag{18}$$

Now we replace the Cartesian coordinate (z,δ) with the action-angle coordinate (J,ϕ)

$$\begin{aligned} \Delta P_y(J,\phi) = -\frac{4\pi\epsilon_0 N_b r_0\beta_y}{\gamma}\iint dJ'd\phi'\psi(J') \\ \times Y(J',\phi')W^{\perp}[z(J,\phi)-z'(J',\phi')]. \end{aligned} \tag{19}$$

Perform Fourier expansion on both sides of Eq. (19), multiply by $e^{-il\phi}$, and integrate over ϕ to obtain

$$\Delta P_l(J) = -\frac{\beta_y}{2\pi}\sum_{l'}\int \psi(J')Y_{l'}(J')W^{\perp}_{ll'}(J,J')dJ', \tag{20}$$

where

$$\begin{aligned} W^{\perp}_{ll'}(J,J') = \frac{4\pi\epsilon_0 N_b r_0}{\gamma}\iint d\phi'd\phi\, e^{il'\phi'-il\phi} \\ \times W^{\perp}[z(J,\phi)-z'(J',\phi')]. \end{aligned} \tag{21}$$

Discretize J as done in Sec. II B

$$\Delta P_l(J_k) = -\frac{\beta_y}{2\pi}\sum_{l'}\sum_{k'}\psi(J'_{k'})Y_{l'}(J'_{k'})W^{\perp}_{ll'}(J_k,J'_{k'})\Delta J'_{k'}. \tag{22}$$

The transfer matrix of transverse wakefield for the vector $[Y_l(J_k), P_l(J_k)]$ can be written as

$$M_{\text{wake}} = \begin{bmatrix} 1 & 0 \\ M_{lkl'k'} & 1 \end{bmatrix}, \tag{23}$$

where

$$M_{lkl'k'} = -\frac{\beta_y}{2\pi}\Delta J_{k'}W^{\perp}_{ll'}(J_k,J_{k'})\psi(J_{k'}).$$

Equation (21) can also be constructed from transverse impedance $Z^{\perp}(\omega)$

$$W^{\perp}_{ll'}(J,J') = -i\frac{2\epsilon_0 N_b r_0}{\gamma}\int_{-\infty}^{+\infty} d\omega \cdot Z^{\perp}(\omega) \times \int_0^{2\pi} d\phi' \cdot e^{i[l'\phi' - \omega z'(J',\phi')/c]} \times \int_0^{2\pi} d\phi' \cdot e^{-i[l\phi - \omega z(J,\phi)/c]}. \quad (24)$$

D. Ideal feedback

The bunch-by-bunch feedback system determines the kicks by measuring the bunch's dipole amplitude, while these kicks can only affect the dipole motion of the bunch. The feedback mechanism exhibits dual effects: reactive and resistive feedback [7], which respectively induce tune shift and damping on the bunch's dipole motion. The resistive feedback kick can be written as

$$\Delta P_{\text{resi}} = 2D\int_{-\infty}^{+\infty} P(J',\phi')\psi(J')dJ', \quad (25)$$

where D is the damp rate of resistive feedback. $D > 0$ is damping and $D < 0$ is antidamping. It is worth mentioning that ΔP_{resi} is independent of coordinates J and ϕ, because the ideal feedback applies kicks uniformly to all particles. We perform a Fourier expansion to ϕ on both sides, multiplying by the factor $e^{-il\phi}$, and integrating over ϕ. Equation (25) is derived as

$$\Delta P_{0,\text{resi}} = 4\pi D\int_{-\infty}^{+\infty} P_0(J')\psi(J')dJ'. \quad (26)$$

The subscript 0 denotes $l = 0$. Both sides of the equation relate exclusively to modes of $l = 0$, indicating that the feedback only depends on the $l = 0$ modes and acts only on them. Finally, discretize J to obtain

$$\Delta P_{0,\text{resi}} = 4\pi D\sum_{i=0}^{+\infty} P_0(J'_{k'})\psi(J'_{k'})\Delta J'_{k'}. \quad (27)$$

Similarly, the reactive feedback kick can be expressed as

$$\Delta P_{0,\text{reac}} = 4\pi R\sum_{i=0}^{+\infty} Y_0(J'_{k'})\psi(J'_{k'})\Delta J'_{k'}, \quad (28)$$

where R is the coefficient related to reactive strength. R/π is the tune shift from reactive feedback. The transfer map of feedback for the vector $[Y_l(J_k), P_l(J_k)]$ can be written as

$$M_{\text{fb}} = \begin{bmatrix} 1 & 0 \\ M_{\text{reac},0k'} & 1 - M_{\text{resi},0k'} \end{bmatrix}, \quad (29)$$

$$M_{\text{reac},0k'} = 4\pi R\psi(J'_{k'})\Delta J'_{k'},$$
$$M_{\text{resi},0k'} = 4\pi D\psi(J'_{k'})\Delta J'_{k'}.$$

In this study, we focus on the resistive feedback. As shown in Eq. (29), the feedback mechanism solely depends on and affects the $l = 0$ modes. Therefore, in the transfer matrix of Eq. (29), all matrix elements associated with $l \neq 0$ modes are zero, except for the unit entries on its diagonal.

The total transfer matrix for one revolution is $M_{\text{total}} = M_{\text{arc}}M_{\text{wake}}M_{\text{fb}}$. The stability of the bunch is determined by the eigenvalues λ of M_{total}. The growth rate is $\log|\lambda|$ with unit turn^{-1} and eigentune is $\tan^{-1}(\text{Im}\lambda/\text{Re}\lambda)/(2\pi)$. To capture the richer information in high-density, small-J regions, we use a nonuniform sampling strategy, with dense spacing for small J and sparse for large J. The formula for J_k and ΔJ_k are

$$J_k = \frac{\varepsilon_{z,0}}{2}\left(\frac{k\cdot r_{\max}}{n_J}\right)^2 \qquad \Delta J_k = k\cdot\left(\frac{r_{\max}}{n_J}\right)^2\varepsilon_{z,0}, \quad (30)$$

where n_J is the number of sampling points. $r_{\max}$ defines the maximum sampling range as $r_{\max}\times\sigma_z$ (e.g., $5\sigma_z$ for $r_{\max} = 5$). $\varepsilon_{z,0}$ is the unperturbed longitudinal emittance. The typical values of n_J and $r_{\max}$ are $40\sim50$ and $4\sim5$. If numerous higher-order modes are involved in the instability, larger n_J and $r_{\max}$ are needed.

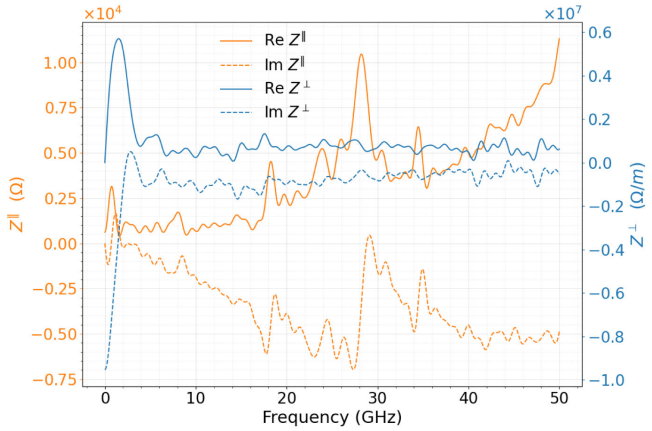
III. THRESHOLD DEPENDENCE ON FEEDBACK AND CHROMATICITY

In this section, we focus on how the instability threshold varies with chromaticity and feedback damping rate under conditions with or without $Z^{\parallel}$, using both simulation and analytical methods. We choose three electron storage rings to investigate this topic: SuperKEKB LER [36], circular electron positron collider (CEPC) [37], and high energy photon source (HEPS) [38]. The parameters of the three machines used in this paper are listed in Table I, and their impedances are shown in Figs. 1(a) [39], 1(b) [40], and 1(c) [41]. Simulation code IBB [34,42,43] is used in this work. IBB is a three-dimensional beam-beam interaction code

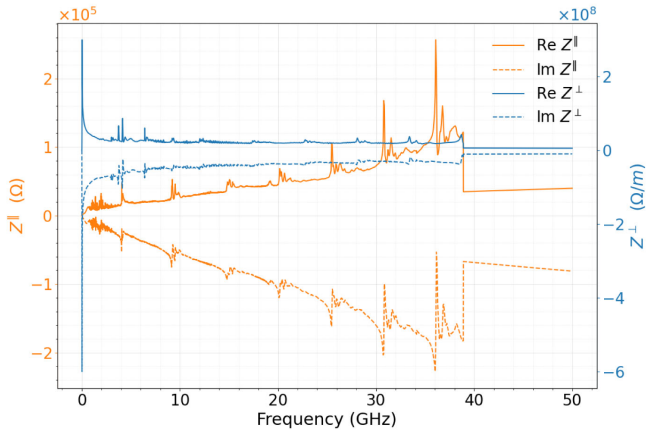
TABLE I. Main machine parameters.

Parameters	SuperKEKB	CEPC[a]	HEPS
Energy E (GeV)	4.0	45.5	6.0
Bunch length σ_z (mm)	4.60	9.63	5.02
Energy spread σ_δ (10^{-4})	7.53	13.6	10.2
Synchrotron tune ν_s	0.023	0.0176	0.00098
Vertical tune ν_y	0.685	0.595	0.290
Circumference (m)	3016	50000	1360
χ/ν_1	0.033	0.077	1.04
Radiation damping time τ_y/τ_z (ms)	45.6/22.8	408/204	20.6/18.7

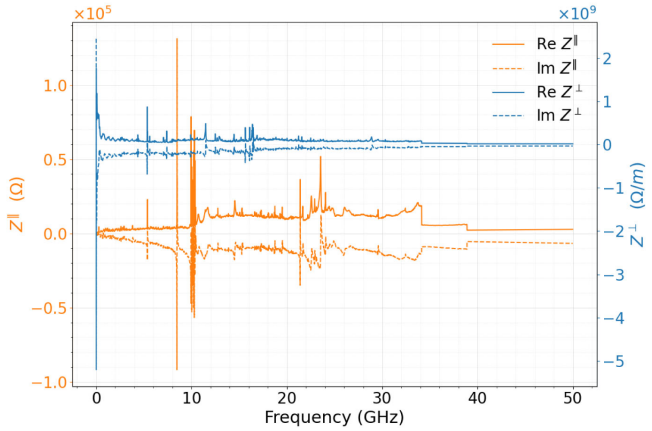
[a]The half-ring model and the beamstrahlung-lengthened bunch length are used.



(a)



(b)



(c)

FIG. 1. Longitudinal and transverse impedance of three machines. (a) SuperKEKB LER, (b) CEPC, and (c) HEPS.

developed for accelerator design and optimization. It can also account for a range of other effects, including longitudinal and transverse impedance, chromaticity, and feedback. We adopt the head-tail phase $\chi = 2\pi\nu_1\sigma_{z,0}/\eta C_0 = \nu_1\sigma_{\delta,0}/\nu_s$ to quantify the chromatic effects, where $\sigma_{z,0}$ and $\sigma_{\delta,0}$ are the unperturbed bunch length and energy spread.

First, we present simulation and analysis results without considering $Z^{\parallel}$. Synchrotron radiation (SR) is included in the simulation. The threshold variations are similar between SuperKEKB [Fig. 2(a)] and CEPC [Fig. 2(b)]. The feedback decreases the threshold at zero chromaticity. When chromaticity is decreased from zero, the threshold first rises and then falls. The achievable threshold never exceeds I_{tmci}. Conversely, as chromaticity is increased from zero, the threshold first decreases, then increases to a maximum before decreasing again. Even with very strong feedback (such as $D \approx 0.05$), the highest attainable threshold cannot greatly exceed I_{tmci} in SuperKEKB. Although the threshold in CEPC can be raised by a factor of 1.4, it requires very strong feedback ($D \approx 0.04$). It appears that combining feedback with a slightly negative chromaticity would be a preferable configuration. The scenario in HEPS is something different, as shown in Fig. 2(c). Feedback raises the threshold at zero chromaticity. When chromaticity is decreased from zero, the threshold tends to decrease directly without any increase. As chromaticity increases from zero, the threshold exhibits a sharp rise at a certain value. With feedback added, it reaches a maximum thereafter and then decreases slowly. In the positive chromaticity regime, the instability threshold can reach up to 2.5 times the value of I_{tmci}. However, whether combined with positive or negative chromaticity, excessively strong feedback (i.e., its damping rate considerably larger than the synchrotron tune, as in the case of $D \approx 0.005$) appears to exhibit saturation, making it difficult to increase the threshold further. It is obvious that feedback can further increase the instability threshold (even at considerably low chromaticity). Simulation also shows that SR can further increase the threshold significantly in all three machines with sufficiently strong feedback and chromaticity.

We now extend the simulation and analysis by incorporating $Z^{\parallel}$. As shown in Figs. 3(a) and 3(b), both SuperKEKB and CEPC exhibit a significant threshold increase within the positive chromaticity region. When the feedback is sufficiently strong (such as $D \approx 0.02$), the threshold nearly doubles in SuperKEKB and reaches 2.5 times the original value in CEPC, with both near $\chi \approx 0.4$. Figure 3(c) shows that the threshold of HEPS even triples at $\chi \approx 0.4$ without feedback and can reach a higher value with feedback. The threshold calculated by the analysis is cut off at around 3.55. This cutoff is necessary because higher beam intensities would induce MWI, thereby making a stable longitudinal equilibrium distribution unattainable and invalidating the theoretical model. In the negative chromaticity regime, none of the three machines exhibits a significant improvement in its threshold, unlike that in the positive chromaticity regime. On the whole, the feedback combined with positive chromaticity holds greater potential for increasing the instability threshold. A curious observation is that SR seems to lose its ability to further increase the threshold as it does without $Z^{\parallel}$.

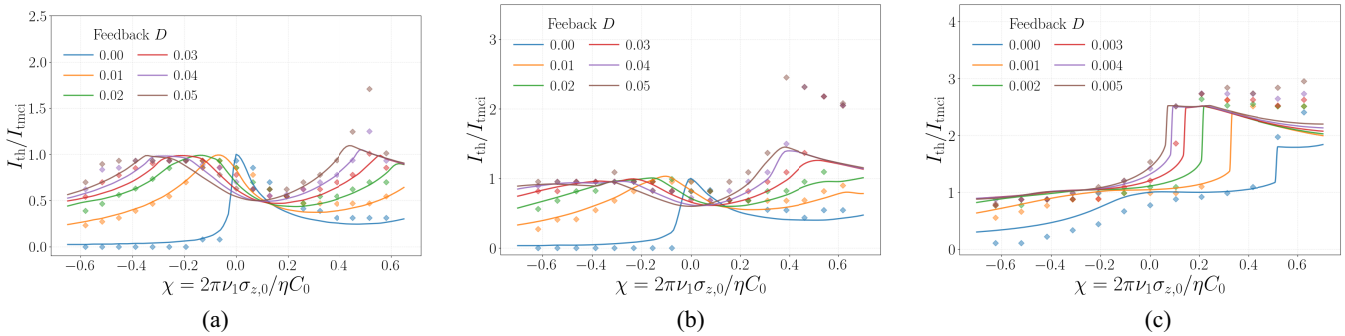


FIG. 2. Instability thresholds versus chromaticity with different feedback configurations in (a) SuperKEKB, (b) CEPC, and (c) HEPS. Simulations and analytical results, which are shown without $Z^{\parallel}$, are represented by diamond markers and solid lines, respectively. Different colors represent different feedback damping rate configurations. All thresholds I_{th} in (a)–(c) are normalized to the threshold I_{tmci} (measured in case without chromaticity, feedback and $Z^{\parallel}$): 2.58 mA for SuperKEKB, 0.14 mA for CEPC, and 0.091 mA for HEPS.

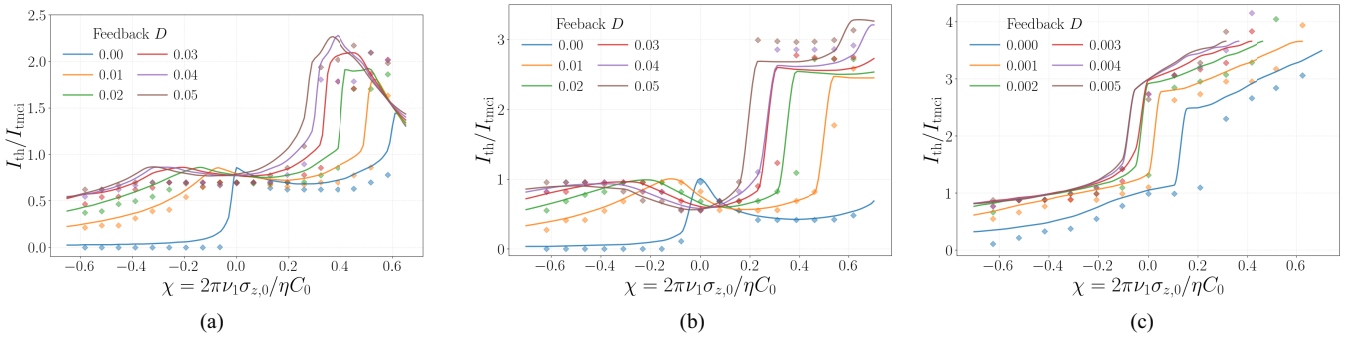


FIG. 3. Same as Fig. 2, but taking the $Z^{\parallel}$ into account. (a) SuperKEKB, (b) CEPC, and (c) HEPS.

Let us now review the conclusions from the existing literature. Theoretical analyses by Karliner and Popov for VEPP-4 and LEP [8] and by Burov for APS and LHC [9], both involving feedback systems, support the existence of higher thresholds in the negative chromaticity regime. In contrast, the analysis by Smaluk *et al.* of NSLS-II [12] reports that using feedback with positive chromaticity is a better choice. As shown in Fig. 2, the optimal configuration differs for each machine when $Z^{\parallel}$ is ignored. When we incorporate $Z^{\parallel}$, the phenomena shown in Fig. 3 become consistent. This finding may explain why a large number of experimental reports prefer the feedback with positive chromaticity [11,12,44–47], as machine experiments inevitably include the effect of $Z^{\parallel}$. A few experiments suggest that higher thresholds within the negative chromaticity regime, operating with feedback damping rates of 0.01–0.02 [10,48]. These results may resemble the case of CEPC as shown in Fig. 3(b): owing to feedback that is not sufficiently strong ($D \approx 0.01$) and a limited chromaticity scan range ($-0.2 < \chi < +0.5$), the maximum achievable threshold remains within the negative chromaticity regime.

The results of this section show that, with $Z^{\parallel}$ included, the instabilities are significantly mitigated when feedback and positive chromaticity are applied. This stabilizing effect is unfeasible within the negative chromaticity regime.

IV. MODES ANALYSIS

We now perform a detailed mode analysis to show how various factors interact in the system. To identify the dominant drivers of the instability, we examine not only the tune shift and growth rate but also the eigenvector of the most unstable eigenmode. Since the underlying physical mechanism is consistent across all three machines, we use SuperKEKB as a representative for the following discussion. The behavior in HEPS exhibits a subtle difference, which is addressed at the end of this section.

We analyze the instability stepwise, first with only transverse impedance as a baseline, then with the addition of longitudinal impedance $Z^{\parallel}$. As shown in Fig. 4(a), the TMCI exhibits a distinct threshold. $Z^{\parallel}$ reduces the tune shift of the coupled mode and induces a distinct tune spread in each $l \neq 0$ mode. The tune spread scales with the azimuthal index l due to the dependence $\nu_y + l\nu_s(J)$. This broadening of the $l = -1$ modes causes them to encounter the mode, which is separated from the $l = 0$ family, at a lower intensity, triggering mode coupling. This phenomenon aligns with the result reported in Ref. [17]. Figure 4(c) shows the eigenvector of the most unstable mode slightly above the intensity threshold. When $Z^{\parallel}$ is introduced, the strongest $l = -1$ oscillation shifts from

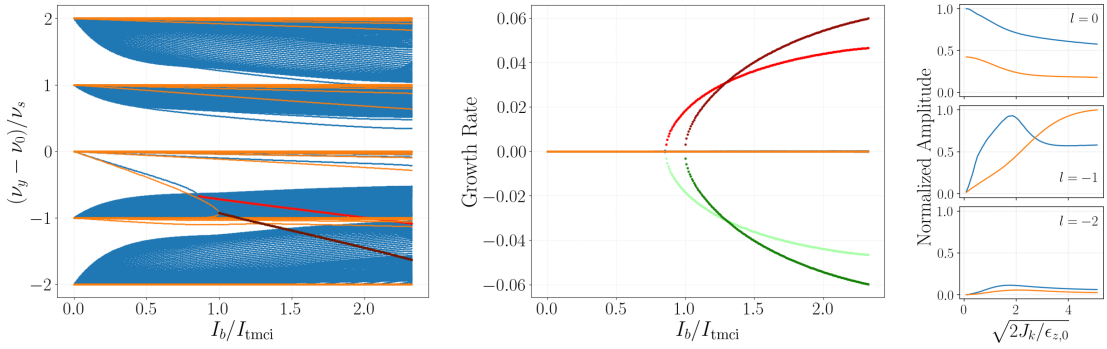


FIG. 4. TMCI tune shift in (a) and growth rate in (b) versus intensity in SuperKEKB. Eigenvector in (c) corresponding to the most unstable eigenmode. Orange (blue) dots denote cases without (with) $Z^{\parallel}$. Dark (light) red and dark (light) green mark the most unstable and most stable eigenmodes without (with) $Z^{\parallel}$, respectively. $I_b/I_{\mathrm{tmci}} = 1.0$ in (c).

being in the large-action region to the small-action region. This phenomenon occurs because small-action $l = -1$ modes possess smaller synchrotron tunes [23,26], which positions them closer to the upper boundary of the $l = -1$ tune spread region (nearer to the $l = 0$ modes) as shown in Fig. 4(a).

Our suppression approach relies critically on feedback. As shown in Fig. 5(a), feedback induces the coupled mode splits into two modes: the one with $l = -1$ is unstable, and the other with $l = 0$ is stable. Simultaneously, Fig. 5(b) shows the emergence of a threshold-less instability. These phenomena match previous studies [6,7]. The eigenvector [Fig. 5(c)] also confirms that the instability is dominated by $l = -1$ modes within low intensity range $(I_b/I_{\mathrm{tmci}} < 1)$. When $Z^{\parallel}$ is introduced, Fig. 5(c) reveals a singular oscillatory $l = -1$ component, manifested as a sharp, isolated "peak" in the eigenvector profile. This profile indicates that while most particles remain with small amplitude oscillation, only a few with specific action oscillate significantly. As the intensity increases, the peak broadens, and more particles oscillate, thereby the instability intensifies [Fig. 5(d)].

Now we examine chromaticity effects in a feedback-free system. Chromaticity splits the coupled mode into two modes, as feedback does. The key difference lies in the stability of the two split modes: for positive chromaticity, the split mode with $l = 0$ is stable, and the $l = -1$ is unstable [Fig. 6(a)]; the opposite holds for negative chromaticity [Fig. 6(e)]. Figures 6(b) and 6(f) indicate that chromaticity can induce head-tail instability. Notably, the growth rate is substantially higher for negative than for positive chromaticity. When $Z^{\parallel}$ is introduced, a singular oscillatory component appears in the eigenvector for positive chromaticity [Fig. 6(c)], but is absent for negative chromaticity [Fig. 6(g)]. This implies that the stabilizing influence of $Z^{\parallel}$ is confined to the positive chromaticity regime. As the intensity increases, the eigenvector for positive chromaticity loses its singular character [Fig. 6(d)]. Conversely, the eigenvector for negative chromaticity [Fig. 6(h)] comes to resemble that in the

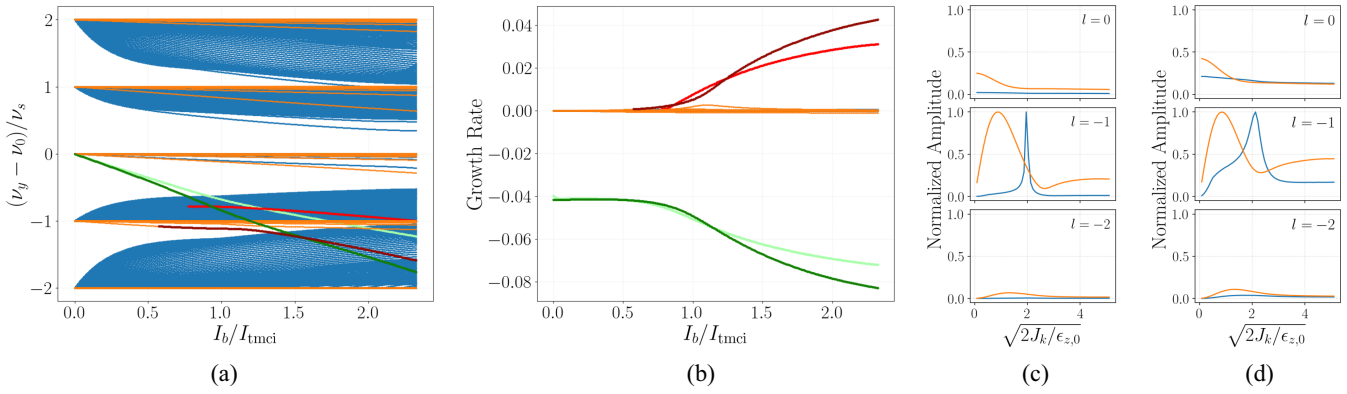


FIG. 5. Feedback with $D = 0.04$ is applied. (a) and (b) show tune and growth rate variation versus intensity, eigenvector (c) and (d) corresponding to the most unstable eigenmode at different intensity. The color scheme for the data points follows the same convention as in Fig. 4. $I_b/I_{\mathrm{tmci}} = 0.65$ in (c) and $I_b/I_{\mathrm{tmci}} = 0.93$ in (d).

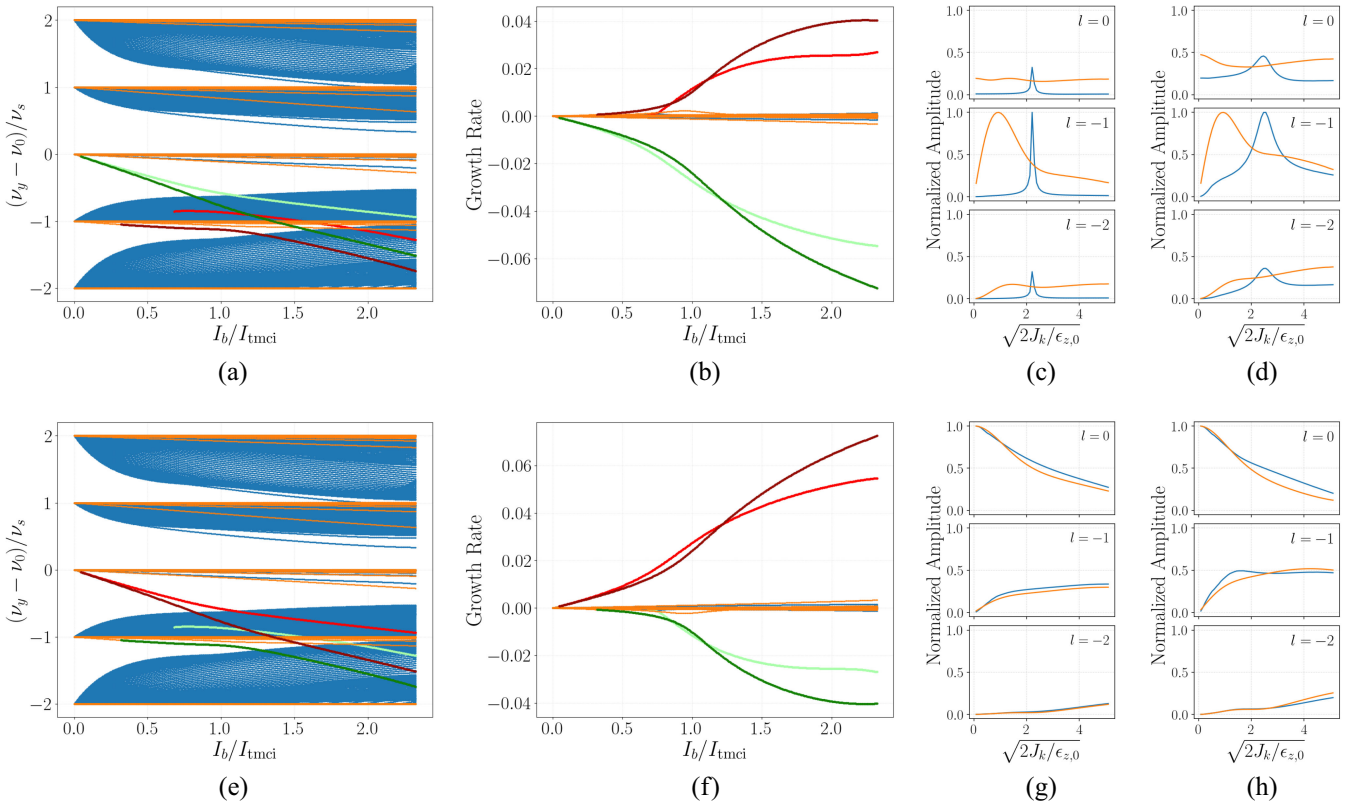


FIG. 6. Same as Fig. 4, but without feedback, and chromaticity is included. $\chi = +0.264$ in (a)–(d) and $\chi = -0.264$ in (e)–(h); $I_b/I_{\mathrm{tmci}} = 0.50$ in (c) and (g); $I_b/I_{\mathrm{tmci}} = 0.89$ in (d) and (h).

pure TMCI case (Fig. 4), indicating that the dominant instability mechanism reverts to mode coupling.

We now consider the case with both feedback and chromaticity. In this combined regime, the coupled mode splits, as shown in Figs. 7(a) and 7(d). For positive chromaticity, the instability growth rate drops from ∼0.06 [Fig. 4(b)] to ∼0.02 [Fig. 7(b)] and is further suppressed below 0.01 when $Z^{\parallel}$ is added, along with a significant increase in the instability threshold. In contrast, for negative chromaticity, the growth rate remains persistently high at ∼0.06 [Fig. 7(e)], and no similar stabilization is observed. This divergence can be understood from the eigenvectors. A sharp peak, indicative of only a singular unstable component, is present in the eigenvector for positive chromaticity [Fig. 7(c)] but absent for negative chromaticity [Fig. 7(f)]. This suggests that $Z^{\parallel}$ can introduce a stabilizing effect specifically for positive chromaticity, effectively raising the instability threshold. For combining negative chromaticity and feedback, the head-tail instability (or feedback-driven) instability below $I_b/I_{\mathrm{tmci}} \sim 1$ is mitigated. However, the instability above $I_b/I_{\mathrm{tmci}} \sim 1$ is still robust.

By examining all instances where $Z^{\parallel}$ introduces a stabilizing effect, we can identify some common features. A noticeable stabilizing effect from $Z^{\parallel}$ tends to occur when the instability is driven by $l \neq 0$ modes primarily. In contrast, when the instability is dominated by the $l = 0$ mode, or when the contributions from $l = 0$ and $l \neq 0$ modes are comparable, $Z^{\parallel}$ struggles to provide stabilization. This difference is easily understood because $Z^{\parallel}$ introduces a tune spread only for $l \neq 0$ modes, leaving the $l = 0$ mode unaffected. Both positive chromaticity and feedback suppress the $l = 0$ components of the instability, forcing the $l \neq 0$ modes to dominate. Such a shift in mode dominance enables the tune spread induced by $Z^{\parallel}$ to become effective, thus leading to a notable increase in the instability threshold. The isolated peak in the eigenvector profile linked to the stabilizing effect of $Z^{\parallel}$, according to Ref. [35], corresponds to a weak artificial growth rather than a real instability. On the other hand, the combination of negative chromaticity and feedback only allows their effects to cancel each other out: feedback drives the $l = -1$ mode while negative chromaticity suppresses it, and negative chromaticity drives the $l = 0$ mode while feedback suppresses it. As a result, the physical picture of the instability degenerates to that of TMCI-like, and $Z^{\parallel}$ exerts its detrimental effect as usual.

The behavior in HEPS differs slightly. Figure 2 demonstrates that feedback and positive chromaticity exert a more pronounced beneficial effect on threshold in HEPS than in CEPC or SuperKEKB. This is because in HEPS, the growth rate of TMCI within the studied intensity range and the radiation damping rate differ by only about one order of

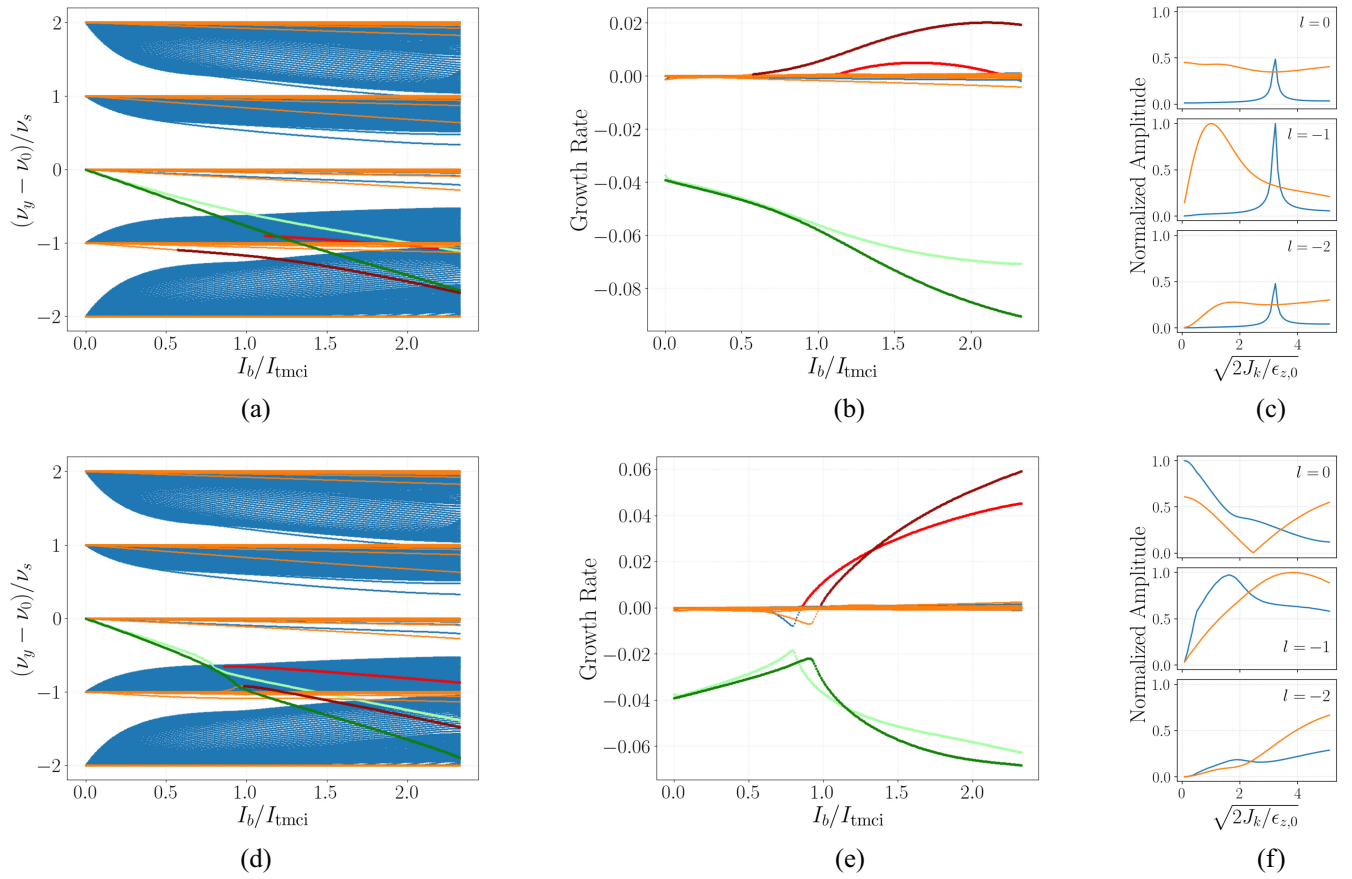


FIG. 7. Same as Fig. 4, but for feedback $D = 0.04$ and chromaticity. $\chi = +0.264$ in (a)–(c); $\chi = -0.264$ in (d)–(f); $I_b/I_{\mathrm{tmci}} = 1.14$ in (c) and (f).

magnitude. As shown in Fig. 8, the TMCI growth rate within the intensity range of interest is on the order of 0.001, an order of magnitude slower than the rates in SuperKEKB and CEPC. Feedback with $D = 0.003$ or slight positive chromaticity $\nu_1 = 0.5$ ($\chi \sim 0.6$) readily suppresses the instability, reducing its growth rate to the level of the synchrotron radiation damping rate ($\sim 10^{-4}$).

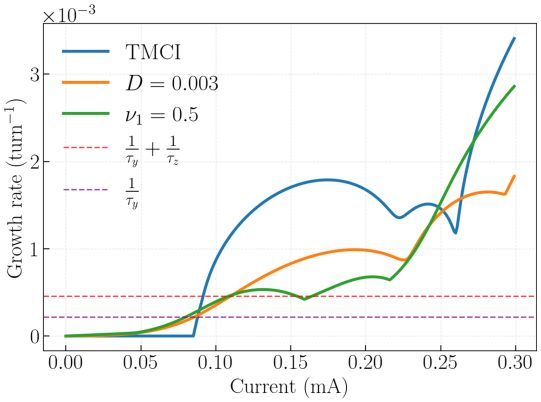


FIG. 8. Growth rate versus bunch current in HEPS. τ_y and τ_z are transverse and longitudinal radiation damping times, respectively.

Therefore, these measures do not lower but slightly increase the instability threshold.

V. SUMMARY AND OUTLOOK

This study presents a theoretical framework for transverse single-bunch instability that incorporates $Z^{\parallel}$, feedback, and chromaticity. Within this framework, the suppression of instabilities due to the combined action of these effects is investigated. When studied separately, longitudinal impedance, feedback, and chromaticity each tend to lower the threshold or even excite threshold-less instability. However, when acting together, they could suppress the instability. The stabilization mechanism can be described as follows: When the instabilities are dominated by $l \neq 0$ modes, the azimuthal tune spread induced by $Z^{\parallel}$ can exhibit a stabilizing effect. The feedback combined with positive chromaticity can suppress the $l = 0$ mode while exciting the $l \neq 0$ mode, thereby the stabilizing effect of the azimuthal tune spread could work. This result may help explain the longstanding discrepancy between theoretical analyses and experimental studies regarding the optimal combination of feedback and chromaticity. Since the azimuthal tune spread is induced by the imaginary part of the longitudinal impedance [17], its

stabilizing effect can be modulated by optimizing the inductive or capacitive component of the impedance. Based on our analysis, a larger azimuthal tune spread is expected to exhibit a stronger stabilizing effect. In future circular accelerator designs, increasing the head-tail phase per chromaticity would enable more effective utilization of the stabilization mechanism discussed in this paper.

ACKNOWLEDGMENTS

This work is supported by the National Natural Science Foundation of China (Grant No. 12475160) and the Chinese Academy of Sciences President's International Fellowship Initiative (Grant No. 2024PVA0057).

DATA AVAILABILITY

The data that support the findings of this article are openly available [36–41].

[1] A. W. Chao, *Physics of Collective Beam Instabilities in High Energy Accelerators*, Wiley Series in Beam Physics and Accelerator Technology (Wiley, New York, 1993).

[2] K.-Y. Ng, *Physics of Intensity Dependent Beam Instabilities* (World Scientific, Hackensack, NJ, 2006), oCLC: ocm66900727.

[3] E. Métral, General mitigation techniques for coherent beam instabilities in particle accelerators, Eur. Phys. J. Plus **137**, 47 (2022).

[4] Y. H. Chin, A. W. Chao, M. M. Blaskiewicz, and Y. Shobuda, Chromaticity effects on head-tail instabilities for broadband impedance using two particle model, Vlasov analysis, and simulations, Phys. Rev. Accel. Beams **20**, 071003 (2017).

[5] V. V. Danilov and E. A. Perevedentsev, Feedback system for elimination of the transverse mode coupling instability, Nucl. Instrum. Methods Phys. Res., Sect. A **391**, 77 (1997).

[6] E. Métral, Imaginary tune split and repulsion single-bunch instability mechanism in the presence of a resistive transverse damper and its mitigation, Phys. Rev. Accel. Beams **24**, 041003 (2021).

[7] K. Ohmi, H. Fukuma, T. Ishibashi, S. Terui, M. Tobiyama, and D. Zhou, Study for −1 mode instability in SuperKEKB low energy ring, in *Proceedings of the 65th ICFA Advanced Beam Dynamics Workshop on High Luminosity Circular e^+e^- Colliders (eeFACT2022), Frascati, Italy* (JACoW, Geneva, Switzerland, 2023), pp. 119–124, 10.18429/JACoW-eeFACT2022-WEXAT0102.

[8] M. Karliner and K. Popov, Theory of a feedback to cure transverse mode coupling instability, Nucl. Instrum. Methods Phys. Res., Sect. A **537**, 481 (2005).

[9] A. Burov, Efficiency of feedbacks for suppression of transverse instabilities of bunched beams, Phys. Rev. Accel. Beams **19**, 084402 (2016).

[10] L. Arnaudon, S. Myers, R. Olsen, and E. Peschardt, Transverse feedback and LEP performance, Conf. Proc. C **920324**, 66 (1992), https://proceedings.jacow.org/e92/PDF/EPAC1992_0066.PDF.

[11] V. Smaluk, D. Sukhanov, V. Oreshonok, V. Cherepanov, and V. Kiselev, Feedback for suppression of single-bunch transverse instability in electron-positron storage rings, J. Instrum. **7**, P01007

[12] V. Smaluk, G. Bassi, A. Blednykh, and A. Khan, Combined effect of chromaticity and feedback on transverse head-tail instability, Phys. Rev. Accel. Beams **24**, 054401 (2021).

[13] P. Kernel, R. Nagaoka, J. L. Revol, and G. Besnier, High current single bunch transverse instabilities at the ESRF: A new approach, in *Proceedings of European Particle Accelerator Conference (EPAC 2000), Vienna, Austria* (JACoW, Geneva, Switzerland, 2000), pp. 1133–1135, https://proceedings.jacow.org/e00/PAPERS/WEP4B04.pdf.

[14] M. Migliorati, C. Zannini, C. Antuono, D. Gibellieri, M. Zobov, M. Behtouei, R. Soos, and Y. Zhang, Studies and mitigation of TMCI in FCC-ee, in *Proceedings of the 15th International Particle Accelerator Conference (IPAC2024), Nashville, TN* (JACoW, Geneva, Switzerland, 2024), THPC60, 10.18429/JACoW-IPAC2024-THPC60.

[15] M. Migliorati, C. Antuono, E. Carideo, Y. Zhang, and M. Zobov, Impedance modelling and collective effects in the future circular e^+e^- collider with 4 IPs, EPJ Tech. Instrum. **9**, 10 (2022).

[16] E. Carideo, F. Zimmermann, M. Zobov, and M. Migliorati, FCC-ee collective effects and their mitigation, Proc. Sci. ICHEP2022 (**2022**) 046.

[17] H.-S. Xu, C.-T. Lin, N. Wang, J.-Y. Xu, and Y. Zhang, Transverse mode-coupling instability with longitudinal impedance, Nucl. Sci. Tech. **35**, 103 (2024).

[18] E. Métral and M. Migliorati, Longitudinal and transverse mode coupling instability: Vlasov solvers and tracking codes, Phys. Rev. Accel. Beams **23**, 071001 (2020).

[19] E. Métral and G. Rumolo, Simulation study on the beneficial effect of linear coupling for the transverse mode coupling instability in the CERN super proton synchrotron, in *Proceedings of European Particle Accelerator Conference (EPAC 2006), Edinburgh, Scotland* (2006), p. 2916, https://proceedings.jacow.org/e06/PAPERS/THPCH058.pdf.

[20] T. Zolkin, A. Burov, and B. Pandey, Transverse mode-coupling instability and space charge, Phys. Rev. Accel. Beams **21**, 104201 (2018).

[21] K. Ohmi, N. Kuroo, K. Oide, D. Zhou, and F. Zimmermann, Coherent beam-beam instability in collisions with a large crossing angle, Phys. Rev. Lett. **119**, 134801 (2017).

[22] N. Kuroo, K. Ohmi, K. Oide, D. Zhou, and F. Zimmermann, Cross-wake force and correlated head-tail instability in beam-beam collisions with a large crossing angle, Phys. Rev. Accel. Beams **21**, 031002 (2018).

[23] C. Lin, K. Ohmi, and Y. Zhang, Coupling effects of beam-beam interaction and longitudinal impedance, Phys. Rev. Accel. Beams **25**, 011001 (2022).

[24] K. Ohmi, L. Huang, H. Liu, and L. Rao, Space charge effects on coupled-bunch instability in high-intensity proton rings, Phys. Rev. Accel. Beams **28**, 070101 (2025).

[25] K. Ohmi and Y. Zhang, Effects of space charge force on the beam-beam mode coupling instability, Phys. Rev. Accel. Beams **27**, 101001 (2024).

[26] Y. Cai, Linear theory of microwave instability in electron storage rings, Phys. Rev. ST Accel. Beams **14**, 061002 (2011).
[27] J. Haïssinski, Exact longitudinal equilibrium distribution of stored electrons in the presence of self-fields, Il Nuovo Cimento B **18**, 72 (1973).
[28] R. Warnock and K. Bane, Numerical solution of the Haïssinski equation for the equilibrium state of a stored electron beam, Phys. Rev. Accel. Beams **21**, 124401 (2018).
[29] R. Warnock and M. Venturini, Equilibrium of an arbitrary bunch train in presence of a passive harmonic cavity: Solution through coupled Haïssinski equations, Phys. Rev. Accel. Beams **23**, 064403 (2020).
[30] T. He, W. Li, Z. Bai, and L. Wang, Numerical solution of the coupled Haïssinski equations for the equilibrium state of an arbitrary bunch train in an electron storage ring, Nucl. Instrum. Methods Phys. Res., Sect. A **1006**, 165434 (2021).
[31] K. Oide and K. Yokoya, Longitudinal single-bunch instability in electron storage rings, https://cds.cern.ch/record/208816/ (1990).
[32] K. Oide, A mechanism of longitudinal single-bunch instability in storage rings, Part. Accel. **51**, 43 (1995), https://inspirehep.net/files/c68532571e82719dad511ab5f1e4ee76.
[33] P. Kicsiny, D. Zhou, X. Buffat, T. Pieloni, and M. Seidel, Incoherent horizontal emittance growth due to the interplay of beam-beam interaction and longitudinal wakefield in crab-waist colliders, Phys. Rev. Accel. Beams **28**, 051002 (2025).
[34] Y. Zhang, N. Wang, K. Ohmi, D. Zhou, T. Ishibashi, and C. Lin, Combined phenomenon of transverse impedance and beam-beam interaction with large Piwinski angle, Phys. Rev. Accel. Beams **26**, 064401 (2023).
[35] K. Ohmi, Y. Zhang, and C. Lin, Beam-beam mode coupling in collision with a crossing angle, Phys. Rev. Accel. Beams **26**, 111001 (2023).
[36] K. Akai, K. Furukawa, and H. Koiso, SuperKEKB collider, Nucl. Instrum. Methods Phys. Res., Sect. A **907**, 188 (2018).
[37] CEPC Study Group, CEPC technical design report–accelerator (v2), arXiv:2312.14363.
[38] Y. Jiao, G. Xu, X.-H. Cui, Z. Duan, Y.-Y. Guo, P. He, D.-H. Ji, J.-Y. Li, X.-Y. Li, C. Meng, Y.-M. Peng, S.-K. Tian, J.-Q. Wang, N. Wang, Y.-Y. Wei, H.-S. Xu, F. Yan, C.-H. Yu, Y.-L. Zhao, and Q. Qin, The HEPS project, J. Synchrotron Radiat. **25**, 1611 (2018).
[39] T. Ishibashi and D. Zhou, Impedance data repository, https://kds.kek.jp/event/40318/.
[40] N. Wang, Y. Zhang, H. S. Xu, Y. D. Liu, J. T. Li, C. T. Lin, Y. T. Wang, H. J. Zheng, and J. Y. Zhai, Impedance driven collective effects in CEPC, J. Instrum. **19**, P02016 (2024).
[41] N. Wang, H. Xu, S. Tian, Z. Duan, and X. Li, Study of beam coupling impedance and beam collective effect in high energy photon source, At. Energy Sci. Technol. **53**, 1601 (2019).
[42] Y. Zhang, K. Ohmi, and L. Chen, Simulation study of beam-beam effects, Phys. Rev. ST Accel. Beams **8**, 074402 (2005).
[43] Y. Zhang, N. Wang, C. Lin, D. Wang, C. Yu, K. Ohmi, and M. Zobov, Self-consistent simulations of beam-beam interaction in future e^+e^- circular colliders including beamstrahlung and longitudinal coupling impedance, Phys. Rev. Accel. Beams **23**, 104402 (2020).
[44] R. Nagaoka, Collective effects at SOLEIL, https://indico.cern.ch/event/459623/contributions/1131140/attachments/1226267/1795307/Nagaoka_FacilityTalk_SOLEIL.pdf (2016).
[45] E. Koukovini-Platia, R. Bartolini, A. Morgan, and G. Rehm, Study of single bunch instabilities with transverse feedback at diamond, in *Proceedings of the 8th International Particle Accelerator Conference (IPAC2017), Copenhagen, Denmark* (JACoW, Geneva, Switzerland, 2017), 10.18429/JACoW-IPAC2017-THPVA029.
[46] J. Jacob, P. Kernel, R. Nagaoka, J. L. Revol, A. Ropert, and G. Besnier, Experimental and theoretical studies of transverse single bunch instabilities at the ESRF, in *Proceedings of the 6th European Particle Accelerator Conference (EPAC 98)* (JACoW, Geneva, Switzerland, 1998), pp. 999–1001, https://proceedings.jacow.org/e98/PAPERS/THP05G.PDF.
[47] J. L. Revol and E. Plouviez, Diagnostics and equipments for single bunch operation at ESRF, in *Proceedings of the 4th European Particle Accelerator Conference* (JACoW, Geneva, Switzerland, 1995), pp. 1506–1508, https://proceedings.jacow.org/e94/PDF/EPAC1994_1506.PDF.
[48] K. Wille and S. Patzold, Damping of coherent transverse oscillations in PETRA, IEEE Trans. Nucl. Sci. **26**, 3281 (1979).